Validation of the WRF regional climate model over the subregions of Southeast Asia: climatology and interannual variability

Satyaban B. Ratna[1,*]**, J. V. Ratnam**[1]**, S. K. Behera**[1]**, Fredolin T. Tangang**[2]**, T. Yamagata**[1]

[1]**Application Laboratory, JAMSTEC, 3173-25 Showa-machi, Kanazawa-ku, Yokohama, Kanagawa, 236-0001, Japan**
[2]**School of Environmental and Natural Resource Sciences, Faculty of Science and Technology, the National University of Malaysia, Malaysia**

ABSTRACT: This study investigates the capability of a regional climate model in simulating the climate variability over Southeast Asia (SE Asia). The present-day climate, covering the period 1991 to 2015, was dynamically downscaled using the Weather Research and Forecasting (WRF) model with a horizontal resolution of 27 km. The initial and boundary conditions for the WRF model is provided with the European Centre for medium-range weather forecasting (ECMWF) reanalysis (ERA-Interim) data. The model reproduced the mean precipitation climatology as well as the annual cycle. Nevertheless, the model overestimated the boreal summer precipitation over the SE Asian mainland, and underestimated the boreal winter precipitation over the Indonesian region. Model biases are associated with the bias in simulating the vertically integrated moisture fluxes. At an interannual scale, the model shows good performance over the SE Asian mainland and the Philippines in all seasons except for the boreal summer. The influence of El Niño/Southern Oscillation (ENSO) on rainfall over mainland SE Asia and the Philippines during JJA is weak, and the model successfully simulated the weak relationship realistically. In contrast, model inter-annual variability over the Indonesia region is good only in boreal summer and autumn seasons. This is because the model successfully simulated the significant negative correlation between rainfall and ENSO. The influence of the Indian Ocean Dipole (IOD) is seen only in the boreal autumn over the Indonesian region, and the model reproduced it reasonably well. The improvement in the representation of precipitation anomaly associated with ENSO/IOD is due to reasonably accurate simulation of large-scale circulation over SE Asia.

KEY WORDS: Downscaling · Regional climate model · WRF · Southeast Asia · ENSO · IOD

1. INTRODUCTION

Southeast Asia (hereafter SE Asia) is characterized by complex terrain and land–water contrasts with major river systems, tropical forests, and many islands. It rests between the waters of the Indian Ocean in the west and the Pacific Ocean in the east. It contains a mainland section to the north (Myanmar, Cambodia, Laos, Thailand, Peninsular Malaysia, and Vietnam – known as the mainland SE Asia) and a maritime section to the south (Brunei, the Philippines, Singapore, East Malaysia, East Timor, Papua New Guinea and Indonesia — known as the Maritime SE Asia) (Fig. 1a).

The climate of SE Asia, and especially maritime SE Asia is mainly tropical: hot and humid all year round with abundant rainfall. The SE Asian region lies in the range of the classical tropical monsoons (Zeng & Zhang 1998, Li & Zeng 2005), which is surrounded by the positions of the Intertropical Convergence Zone

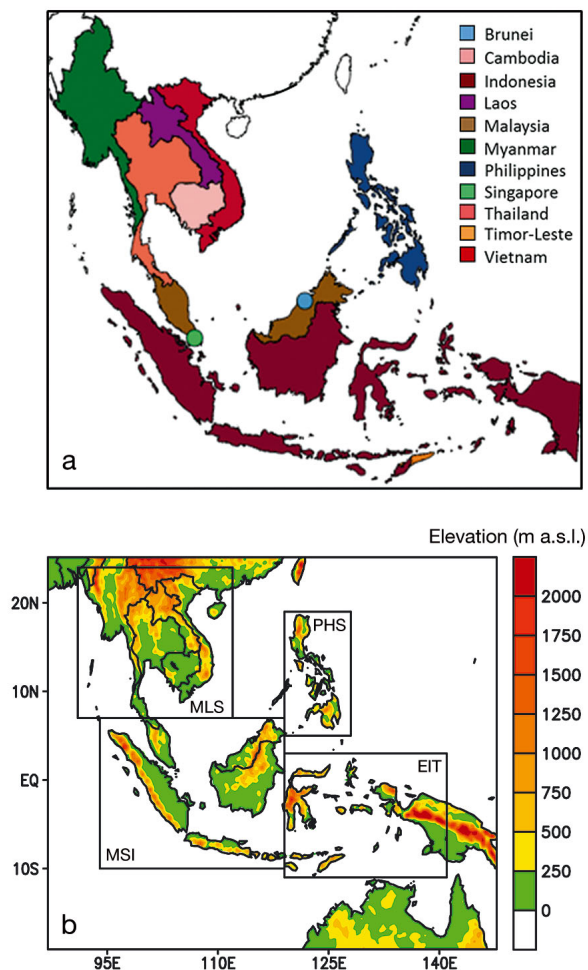*Corresponding author: satyaban@jamstec.go.jp

Fig. 1. (a) Southeast Asia with country boundaries; (b) WRF model domain with a 27 km horizontal grid resolution used in this study. Topography (expressed in meters above mean sea level) is shaded. The 4 boxes in (b) are the sub-regions of Southeast Asia considered in this study for the model validation (see Fig. 2 for definitions)

(ITCZ) in summer and winter. The majority of the SE Asia region is influenced by seasonal shifts in winds or the monsoon, and much of the region is annually affected by extreme weather events, particularly tropical cyclones, droughts, and floods (Yusuf & Francisco 2009). During some years, rainfall over SE Asia region is altered by large-scale conditions associated with El Niño/Southern Oscillation (ENSO) and Indian Ocean dipole (IOD) events (e.g. Kripalani & Kulkarni 1997, McBride et al. 2003, Tangang & Juneng 2004, Naylor et al. 2007, Behera et al. 2008, Ummenhofer et al. 2013, Salimun et al. 2014). The influence of large-scale climate phenomena varies across the region due to orography and ocean–atmosphere interactions. Variability in the climate has a great impact on the socioeconomic conditions of the region, and accurate fore-

casting of the weather and climate would be beneficial. However, the climate of SE Asia has not been sufficiently studied to improve the seasonal forecasts over the region.

Despite the development of many global general circulation model (GCM) systems for seasonal forecasts, the skill of the models in forecasting precipitation is still a challenge. Recenly, Salimun et al. (2014) have suggested that GCMs tend to have lower skill for seasonal rainfall predictions over SE Asia. The poor skill of a GCM in forecasting precipitation is often attributed to low horizontal resolution of the GCM. An important aspect of improving precipitation in GCM simulations is to resolve the regional heterogeneity (Giorgi & Mearns 1999). The technique of dynamical downscaling, wherein a high-resolution regional climate model (RCM) is embedded into a low-resolution GCM output, is often used to improve the simulation of precipitation (e.g. Dickinson et al. 1989, Giorgi 1990, Giorgi et al. 2004). It is assumed that the RCM, due to better representation of regional processes, will improve the GCM simulated precipitation.

Before using a RCM for the purpose of seasonal forecast using global climate model (GCM) boundary conditions, the fidelity of the RCM in reproducing the observed regional climate is assessed in order to understand the systematic biases in the model. Often, the assessment is carried out by forcing a RCM with observed/reanalysis data (Giorgi & Mearns 1999). In recent years, many attempts have been made to understand regional climate variability over SE Asia using regional climate models (e.g. Aldrian et al. 2004, Francisco et al. 2006, Im et al. 2008, Phan et al. 2009, Takahashi et al. 2009, 2010, Chotamonsak et al. 2011, 2012, Ngo-Duc et al. 2014, Phan et al. 2014, Raktham et al. 2015, Raghavan et al. 2016, Juneng et al. 2016). To the authors' knowledge, there are no comprehensive studies available evaluating the performance of an RCM over SE Asia and its subregions for different seasons of the year. Also, RCM performance has not been fully evaluated with regards to mean climatology, interannual variability, and the relationship of the latter with ENSO and IOD. Past studies are limited either to study of a specific event or a particular season, and over a particular sub-region of SE Asia. In this study, we try to fill the gap by performing a regional model simulation over a relatively long period of 25 yr at a horizontal resolution of 27 km, and evaluating its performance in simulating the precipitation over 4 subregions of SE Asia during boreal summer (June-July-August; JJA), boreal autumn (September-October-November; SON), boreal winter (December-January-February;

DJF), and boreal spring (March-April-May; MAM). The performance of the model is evaluated at seasonal, annual, and interannual time scales.

2. MODEL, METHODOLOGY AND DATA

Advanced Research Weather research and forecasting (WRF) model (ARW) version 3.6.1 (Skamarock et al. 2008), developed by the National Centre for Atmospheric Research (NCAR) and designed to serve both operational forecasting and atmospheric research, is used in this study. The WRF model is a non-hydrostatic, fully compressible, and terrain-following sigma coordinate model. In this study, WRF simulations over SE Asia are performed using a domain with horizontal resolutions of 27 km (Fig. 1b). The model has 32 levels in the vertical with the upper boundary at 10 hPa. The WRF domain covers the SE Asia land mass, as well as parts of the surrounding Pacific and Indian Oceans (19.12° S to 25.15° N, 86.96° to 147.77° E), with 251 grid points in the east–west and 188 grid points in north–south directions. The model analysis is carried out by dividing the SE Asia region into 4 subregions (Fig. 1b): (1) mainland SE Asia (MLS), (2) Malaysia, Singapore, Brunei, western Indonesia (MSI), (3) the Philippines (PHS), and (4) eastern Indonesia (EIT). The regions of MLS and PHS that lie to the north of 5° N receive most of their annual rainfall during the boreal summer. However, the MSI and EIT regions located in the equatorial belt receive rainfall throughout the year except for a reduced amount during the boreal summer. The subregions were chosen based on rainfall variability, and in such a way that the major landmasses can be accommodated in the chosen boxes (Fig. 1b).

Physical parameterization schemes considered in this study include cumulus parameterization schemes of Betts-Miller-Janjic (Betts & Miller 1986, Janjic 1994), the microphysics scheme of the WSM 3-class simple ice scheme (Hong et al. 2004), the Unified NOAH scheme for land surface processes (Chen & Dudhia 2001), the Yonsei University scheme for the planetary boundary layer (Noh et al. 2003), the rapid radiative transfer model (RRTM) scheme for long waves (Mlawer et al. 1997), and the Dudhia scheme for short waves (Dudhia 1989). The first author in an earlier study (Ratna et al. 2014) for the South Africa region also used a similar configuration, and the model shows good skill simulating climatology and interannual variability of rainfall. Recently, Ratna et al. (2016b) evaluated 4 different convection parameterization schemes over SE Asia for a shorter

period of 3 yr, 1990–1993. They found that all convection schemes could reproduce the spatial distribution of rainfall over SE Asia, but the area-averaged rainfall bias with the BMJ scheme was lower compared to that of the other 3 convection schemes. Also, they showed that the annual cycle of precipitation was well simulated by the BMJ scheme with a higher correlation coefficient compared to the other schemes. So, based on Ratna et al. (2014, 2016b), we have used the combination of most suitable parameterization schemes in this study. The WRF model was initialized using the 00:00 h UTC 1 January 1990 data and was integrated up to 00:00 h UTC 1 January 2016 considered in this study. The first year of simulations was regarded as model spin-up and excluded from analysis. The model output data were saved in 6 h intervals, but converted into the monthly mean to study the seasonal climatology and interannual variability.

The 6 hourly, 0.75° × 0.75° grid European Centre for medium-range weather (ECMWF) reanalysis (ERA-Interim) data (Dee et al. 2011) was used as the initial and boundary conditions for the simulations. Sea surface temperatures (SST) from ERA-Interim fields were interpolated to the WRF model grid resolution and used as slowly varying lower boundary input. Surface topography data and 24 category land-use index data based on climatological averages, both at a 30 s resolution, were obtained from the United States Geological Survey (USGS). The NOAA optimum interpolation SST version 2 data (Reynolds et al. 2002) is used to identify the El Niño/La Niña and IOD events. We note that the El Niño and La Niña events in this study for all the seasons are based on the SST anomaly over Niño 3.4 region (5° S to 5° N, 170° to 120° W). The El Niño (La Niña) events are identified when the area-averaged SST anomaly over Niño 3.4 region is above (below) 1 standard deviation for a season during the study period 1991 to 2015. Similarly, the positive (negative) IOD events are defined when an anomalous SST difference between the western equatorial Indian Ocean (10° S to 10° N, 50 to 70° E) and the southeastern equatorial Indian Ocean (10° S to 0° N, 90° to 110°E) is above (below) 1 standard deviation for a season. The mean, standard deviation, and anomaly values for each seasons are calculated with respect to the baseline period 1991—2015. The years identified with ENSO and IOD for different seasons of the year are presented in Table 1.

The large-scale model-simulated parameters in this study are compared with ERA-interim data by interpolating the model data to ERA-Interim grid. To

Table 1. ENSO and IOD years considered here in this study. The years in the DJF correspond to January and February of the given year and December of the previous year

	MAM	JJA	SON	DJF
El Niño	1992, 1993, 1998, 2015	1997, 2002, 2015	1997, 2002, 2015	1992, 1998, 2003, 2010
La Niña	1999, 2000, 2008, 2011	1998, 1999, 2010	1998, 1999, 2007, 2010	1999, 2000, 2008, 2011
+ve IOD	1991, 1994, 2000, 2007, 2009	1994, 1997, 2003, 2008, 2012	1994, 1997, 2006, 2015	1996, 1998, 2001, 2010
−ve IOD	1992, 1996, 2002, 2013	1992, 1996, 1998, 2013, 2014	1992, 1996, 1998, 2010	2005, 2006, 2015

validate the model simulated rainfall with the observed rainfall, the 0.5° Climate Research Unit version 3.24 dataset (CRU; Harris et al. 2014) was used. In a recent study, Ratna et al. (2016b) evaluated various monthly mean precipitation data over Southeast Asia region, such as APHORODITE (Yatagai et al. 2012), GPCP (Adler et al. 2003), and CRU precipitation data for the common period of 1991 to 2007. GPCP and CRU are closer to each other, but APHRODITE shows lower precipitation values over SE Asia. Ratna et al. (2016b) also compared the CRU, GPCP, and TRMM (Huffman et al. 2007) precipitation data for the common period 1998 to 2012 and found that CRU and TRMM are closer to each other and the GPCP data show slightly lower values. Based on the above analysis and also due to the availability of data for the whole period of 1991 to 2015, we have used CRU data in this study. Also, CRU data are widely used for the evaluation of regional climate modelling studies over Southeast Asia (Phan et al. 2009, Chotamonsak et al. 2011, Liew et al. 2014, Raghavan et al. 2016 and others).

3. RESULTS AND DISCUSSION

3.1. Mean rainfall climatology

The annual cycle (based on 25 yr climatology) of monthly mean rainfall for 4 subregions are compared with the WRF simulated rainfall (Fig. 2). Due to seasonal migration of the ITCZ, the peak season of the average monthly rainfall is different among subregions. Precipitation in the MLS region peaks in the months of boreal summer, whereas the MSI region has a peak mostly in the months of boreal winter. The PHS region has a slightly longer rainy season compared to the MLS region, though the peak in both regions are in the

boreal summer period. The seasonality is relatively weak in the EIT region, with slightly higher precipitation in the boreal winter and boreal spring season. Overall, the model simulated a realistic annual cycle in all the subregions. However, the model tends to overestimate (underestimate) the precipitation in the period of high (low) rainfall over different subregions (Fig. 2).

Further analysis of the WRF simulated 25 yr climatology for the spatial distribution of precipitation was carried out at both annual and seasonal scales. For the seasonal scale evaluation, we averaged the precipitation over all the months within a season. The seasonal movement of the ITCZ controls the precipitation over
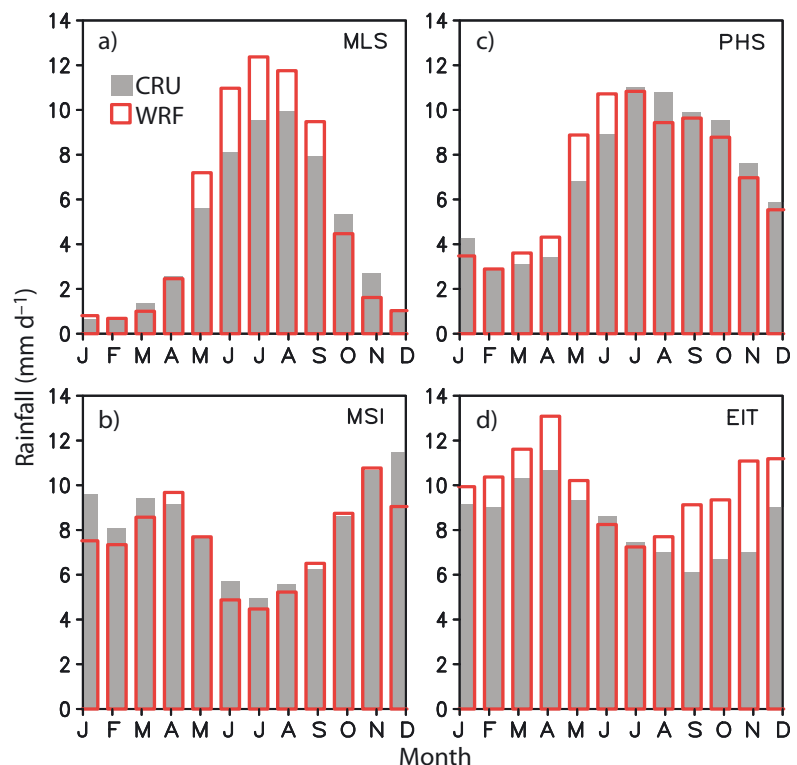

Fig. 2. Annual cycle of the area-averaged rainfall climatology (mm d^{-1}) of the 25 yr (1991–2015) over 4 sub-regions of the Southeast Asia: (a) mainland SE Asia (MLS), (b) Malaysia, Singapore, Brunei, western Indonesia (MSI), (c) the Philippines (PHS) and (d) eastern Indonesia (EIT) both for CRU and WRF

this region. The ITCZ is at the southernmost position in January just near south of the equator; during May, it moves northward to ~5° N, and during July–August, it moves further northward to ~20° N (Matsumoto & Murakami 2002, Lau & Yang 1997).

The observed annual precipitation averaged over the 25 yr period (1991–2015) has high precipitation over the equatorial region (Fig. 3a). A region of high precipitation is also evident over the orographic region of the western coast of the MLS region and in parts of Laos, Vietnam, and the Philippines. The WRF model was able to simulate the north–south rainfall gradient realistically over SE Asia (Fig. 3f). However, the WRF model underestimated precipitation over the western coast of Myanmar, Malaysia, and parts of Kalimantan Island, and overestimated precipitation over eastern parts of MLS, western Sumatra, and the Philippines (Fig. 3k). The model seems to have underestimated the orographic rainfall over the MLS region and overestimated the orographic rainfall over the Indonesian region. The model was also able to capture the spatial variability of the precipitation (Fig. 3g–j) for the different seasons of the year. The model has a dry bias over the region from the equator to 8° N during DJF when maximum annual rainfall occurs (Fig. 3l) During JJA, the maximum annual rainfall occurred over the MLS region when the ITCZ is at its northernmost point, but model simulates large positive bias there (Fig. 3n). The large bias in the precipitation over the MLS region during JJA is also reflected in the annual precipitation bias over the region (Fig. 3k). In the following section, we discuss the mechanism for the simulated precipitation bias in the model.

3.2. Thermodynamic characteristics

To understand the processes that caused the rainfall bias in the WRF simulation, we analyzed vertically integrated moisture convergence and moisture fluxes for the boreal summer and boreal winter season when the biases in the simulated precipitation are largest (Fig. 4). The region north of the equator is a moisture convergence zone during the boreal summer, when the moisture transport occurs from the Bay of Bengal to the MLS region and reaches up to the Philippines as part of the summer monsoon flow (Fig. 4a). The model could simulate the moisture convergence zone, but the simulated moisture convergence is very strong compared to the observation (Fig. 4c). There is a cyclonic circulation of the moisture flux, and the positive bias of moisture conver-

gence (Fig. 4e) extending from eastern MLS to the Philippines contributed to the positive bias of rainfall (Fig. 3n). The southwesterly monsoon wind from the Indian Ocean contributes to the seasonal rainfall over the Myanmar and neighboring zones (Tsai et al. 2015, Ratna et al. 2016a). However, the model simulates a weaker moisture flux transport toward the Myanmar coast compared to the observation, and this has caused the dry bias of rainfall (Fig. 3n). During the DJF season, a moisture convergence region is observed over the region south of 10° N, and moisture transport occurs from the Pacific Ocean (Fig. 4b). However, the model simulates a weaker moisture convergence compared to the observation (Fig. 4d). The weaker moisture convergence is clearly seen in the difference between the model and observations (Fig. 4f). The negative bias of moisture convergence over the region coincides with the dry bias of rainfall (Fig. 3l), especially over Malaysia, eastern Sumatra, and north Kalimantan. In general, biases in the moisture fluxes and their convergence (divergence) as seen in Fig. 4 explain the biases in the spatial distribution of the rainfall (Fig. 3).

To further understand the reasons for the rainfall biases for different seasons and over different subregions of SE Asia, the mean climatology bias of model-simulated vertical profiles of specific humidity and the vertical velocity were analyzed over the MLS and MSI regions by calculating the area-averaged values over the land grid point. The vertical profile analysis is calculated only for the MLS and MSI regions because the model-simulated rainfall shows maximum bias over these 2 regions compared to the other regions (Fig. 3), and this would help to understand the physical processes associated with the model bias. It can be seen from Fig. 3 that only the MLS region has a dominant wet bias during the JJA season, whereas only the MSI region has dominant dry bias during DJF when the maximum annual rainfall occurs over the chosen regions. The vertical profile biases are calculated with respect to the ERA-Interim data. Fig. 5a shows that there is a positive bias of moisture extending from the surface to 300 hPa level during the JJA season over the MLS region. At the same time, there is a positive bias of vertical velocity from the surface to 600 hPa level over MLS region (Fig. 5c). The strong moist atmosphere with strong upward motion in the model during the JJA caused a positive bias of rainfall over MLS region, as seen in Fig. 3n. However, the same region during the DJF season shows low moisture and weak vertical motion compared to the JJA season but still suffers from positive rainfall bias (Fig. 5a,c). The MLS region receives
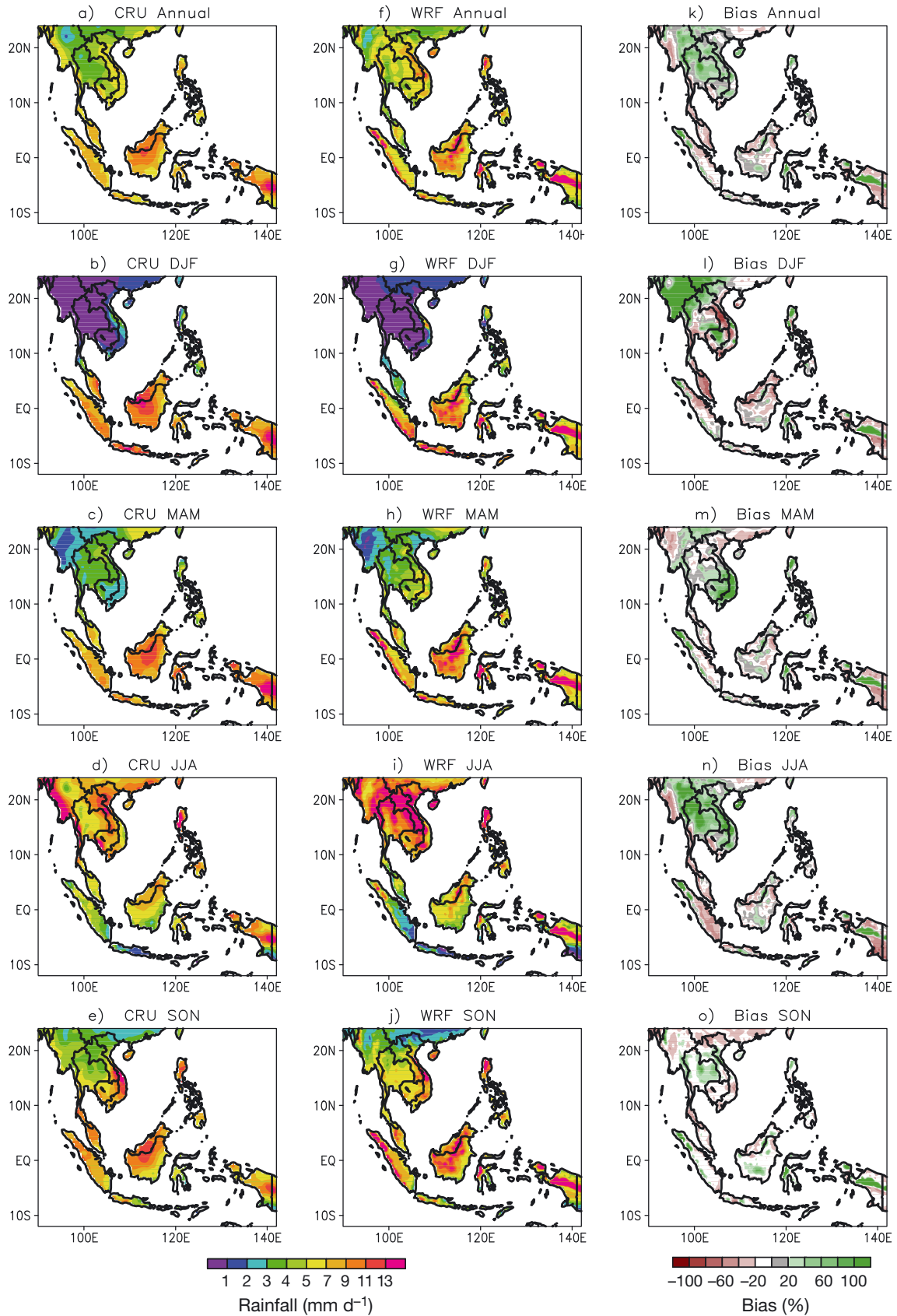
Fig. 3. (a–j) 25 yr (1991–2015) annual and seasonal mean rainfall climatology ([a–e] CRU; [f–j] WRF. (k,l,m,n,o) Same as (a–j), but for WRF bias (%) with respect to CRU

very scanty rainfall during the DJF season, known to be a dry season of the year. In the MSI region, the model simulates a slightly negative bias of moisture from the surface to the 300 hPa level during the DJF season (Fig. 5b). At the same time, the model-simulated vertical velocity is weaker than the ERA-Interim data from the 600 hPa to 150 hPa level (Fig. 5d). These low moisture and weak vertical velocity biases during the DJF season have led to the dry bias of rainfall (Fig. 3l) over the MSI region. However, during the JJA season, the biases of low moisture and weak vertical velocity are smaller compared to those during the DJF season, leading to a small precipitation bias (Fig. 3n).

4. INTERANNUAL VARIABILITY

To employ a regional climate model for short- and longer-term predictions, it is important to determine if the RCM is capable of capturing the observed interannual variability. In this section, we examine the interannual variability simulated by the WRF model for different seasons and for different subregions. The interannual variability of rainfall in terms

of standardized rainfall anomaly for the 4 subregions of MLS, MSI, PHS, and EIT with the seasonal mean rainfall for MAM, JJA, SON, and DJF is analyzed and compared with WRF simulated rainfall (Fig. 6). The observed and WRF seasonal anomalies are calculated based on their respective climatology. The observed and simulated MAM mean rainfall have good correlations for both the MLS and PHS regions, but the correlations are very weak for the MSI and EIT regions (Table 2). During the MAM season, very little rainfall (2 to 5 mm d^{-1}) occurs over the MLS and PHS regions, but more rainfall (6 to 12 mm d^{-1}) occurs over MSI and EIT regions. The correlation for MSI is low, as the model has failed to capture the correct sign of rainfall anomaly for many years where the observed rainfall was above or below 1 standard deviation (Fig. 6a). During JJA, although the model has difficulties in simulating the anomalies in most of the years in the MLS and PHS regions, it does a good job simulating the anomalies in the MSI and EIT regions (Fig. 6b), and this can be seen in terms of correlation value (Table 2). In the SON season, all the regions showed the correct sign of the precipitation anomalies (Fig. 6c) with significant correlations of 0.64, 0.45, 0.69, and 0.80 for the MLS, MSI, PHI, and
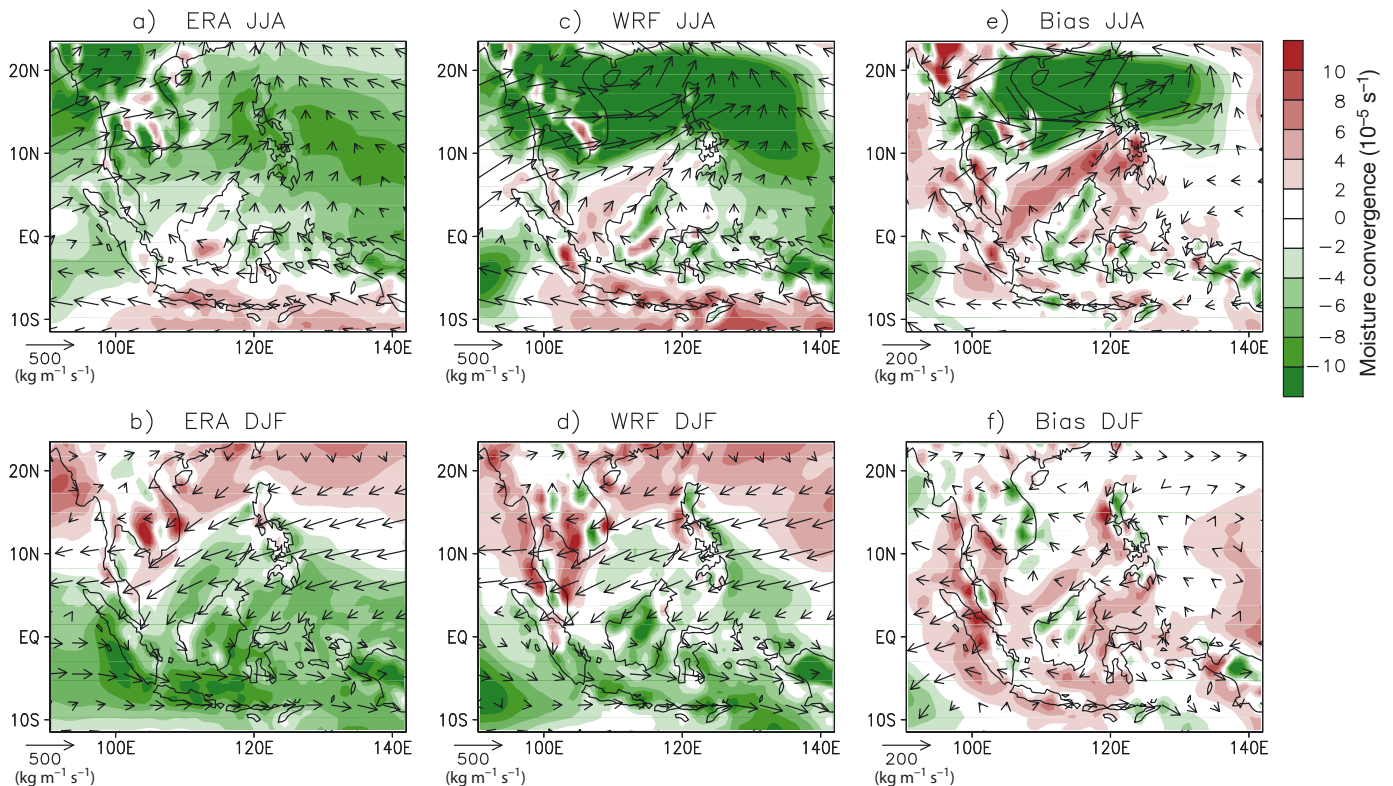

Fig. 4. (a–d) Twenty-five yr (1991–2015) mean climatology of vertically integrated (from 1000 to 300 hPa) moisture convergence and moisture fluxes (arrows) for the JJA and DJF seasons using (a,b) ERA and (c,d) WRF data. (e, f) Same as (a–d), but for bias as calculated from the difference between WRF and ERA
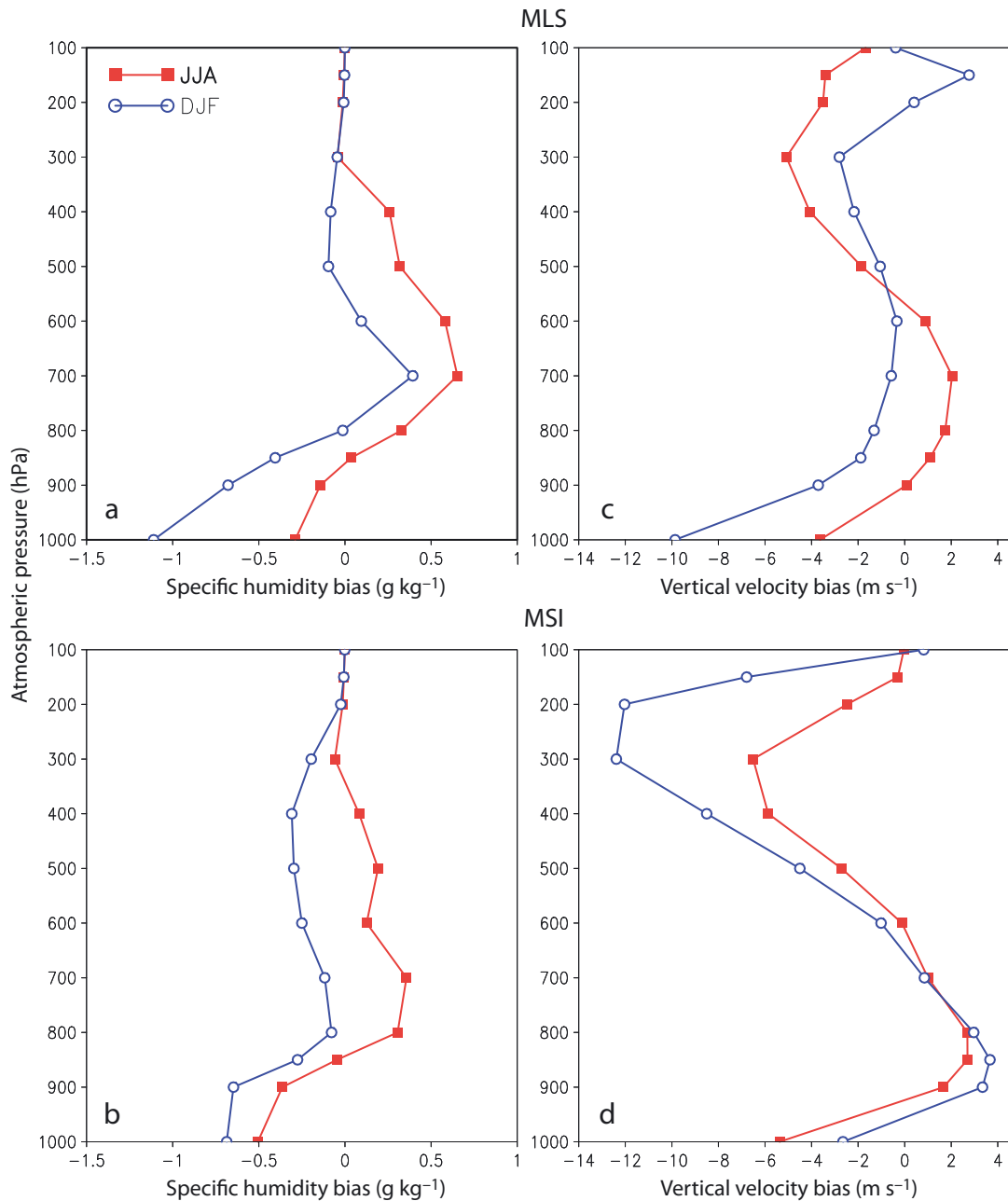
MLS

MSI

Fig. 5. Twenty-five yr (1991–2015) mean climatology bias for the vertical profiles of area-averaged specific humidity and vertical velocity for the JJA and DJF seasons, for (a,c) the MLS and (b,d) MSI regions (see Fig. 2 for definitions). Area averages are calculated over the land grid points, and the model bias is generated relative to ERA interim data

EIT regions, respectively. This is the only season where all the regions have relatively good model performance in terms of interannual variability. During the DJF season, maximum rainfall occurs over the MSI and EIT regions, and there was very little rainfall over the MLS and PHS regions. Here again, we

see the performance of the model for the interannual variability in terms of correlation is poor for the MSI and EIT regions but is good for the MLS and PHS (Table 2) regions.

From the above analysis, it is clear that the model has a systematic precipitation bias during the peak

Fig 6. Interannual variability of standardized precipitation anomaly over 4 sub regions of SE Asia, namely MLS, MSI, PHS and EIT regions (see Fig. 2 for definitions), for the seasons (a) MAM, (b) JJA, (c) SON and d) DJF
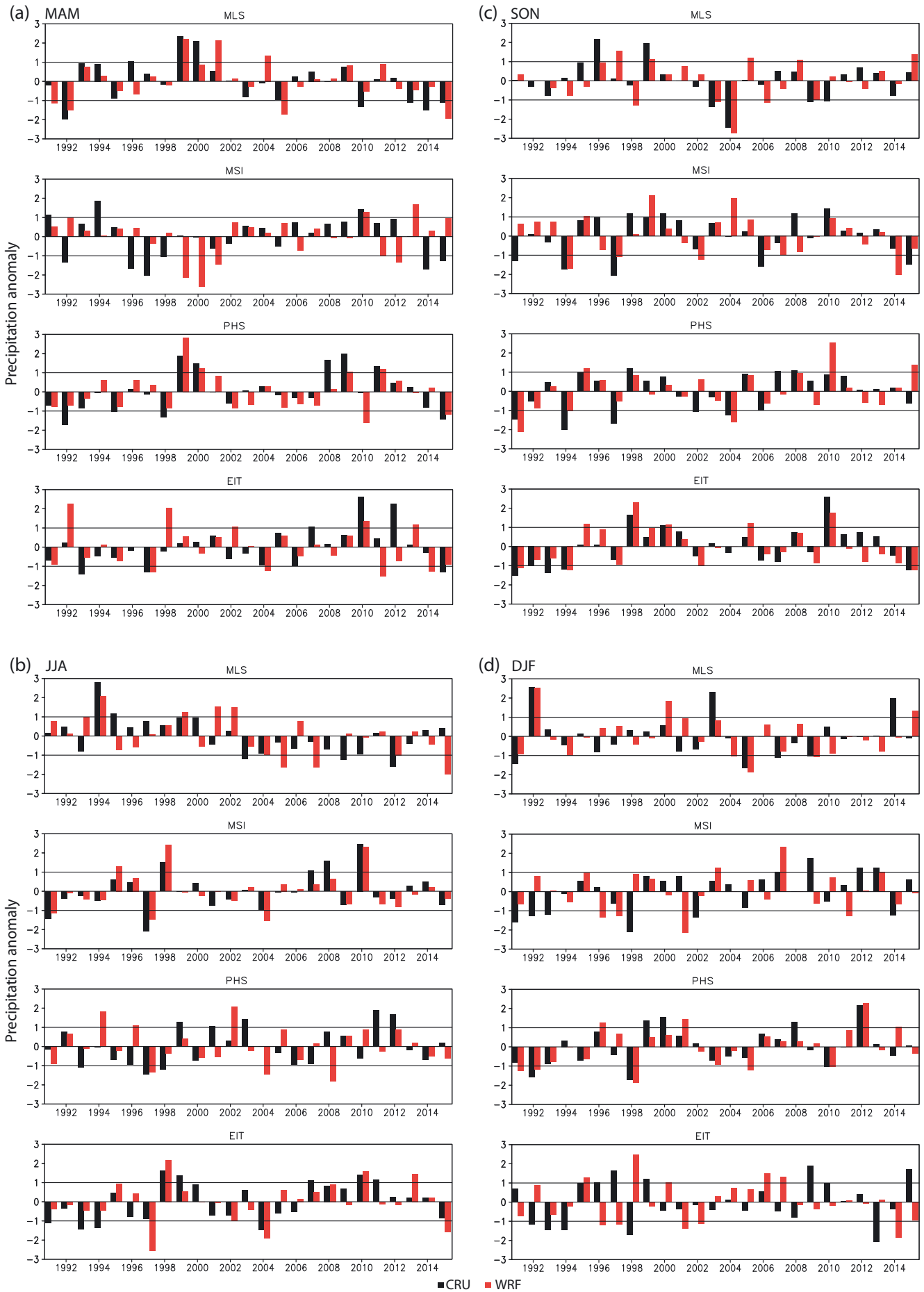
(a) MAM

(b) JJA

(c) SON

(d) DJF

Precipitation anomaly

■ CRU   ■ WRF

Table 2. Time correlation coefficient between observed and simulated rainfall. *Statistically significant at the 95% level with 2-tailed Student's *t*-test

	MAM	JJA	SON	DJF
MLS	0.68*	0.39	0.64*	0.66*
MSI	−0.01	0.88*	0.45*	−0.06
PHS	0.74*	0.12	0.69*	0.84*
EIT	0.31	0.65*	0.80*	−0.33

rainfall seasons. For example, the MLS region receives substantial precipitation during the JJA season, and the model shows a large bias in mean precipitation, while doing a poor job in simulating the interannual variability. After verifying the performance of interannual variability, we tried to check whether the WRF model can simulate the rainfall anomalies associated with large-scale climate modes, such as ENSO and IOD. The tropical climate modes are known to have better predictability owing to the intrinsic nature of ocean-atmosphere coupling. The predictability of the associated regional climate variations also increases during ENSO and IOD years. Therefore, it is interesting to see whether the model can simulate precipitation anomalies correctly during these events. In the following sections, we evaluate the fidelity of the WRF model in simulating the effects of these climate modes by computing the anomaly correlation and event composites. IOD and ENSO events co-occur in some years, and we have included them in both IOD and ENSO composites, as our interest is to see the overall impact rather than the unique behavior of each climate mode in a regional climate model. In an earlier study, Ratna et al. (2014) have already shown the capability of WRF model in simulating rainfall and ENSO relationship over South Africa, and here, we check whether the model performs equally well for the SE Asia region.

4.1. SE Asia rainfall variability and ENSO

To evaluate the effect of ENSO on the subregions of SE Asia, we computed the correlation between the Niño 3.4 index and the precipitation anomalies over different subregions for different seasons. The correlation was computed for both the observed and the model simulated precipitation (Fig. 7, Table 3). In addition, we prepared composites of the precipitation anomaly from the identified years based on the phase of the ENSO (Fig. 7).

During MAM, the precipitation over the MLS and PHS regions is significant and is negatively correlated with ENSO. However, no significant correlation is seen over the MSI and EIT regions (Fig. 7a) in the observations. The WRF model-simulated precipitation also shows similar negative correlation over the MLS and PHS regions like in the observations, but has spurious positive correlations over the MSI and EIT regions (Fig. 7d). A similar pattern emerges when the events are composited based on the identified events (Table 1). In the JJA season, the MSI and EIT regions are significantly negatively correlated to the ENSO index with no significant correlation over the MSL and PHS regions (Fig. 7g). This is also reflected in the composite of the El Niño and La Niña events (Fig. 7 h,i). During El Niño (La Niña), the Indonesia regions receive lower (higher) precipitation, which is in agreement with Juneng & Tangang (2005). The simulated rainfall anomaly over MLS in JJA is not accurate with respect to ENSO events. This may be the reason the model reproduces weak interannual rainfall variability compared to the observed variability. The influence of ENSO on the MLS region during SON is similar to that of the JJA season, which does not have significant correlation with the Niño 3.4 SST (Fig. 7m). However, the other 3 regions—PHS, MSI, and EIT—have negative correlations with ENSO (Fig. 7m). However, the model-simulated rainfall correlation with ENSO over these 3 regions is low and less significant compared to the observations (Fig. 7p). So, the model produces a weaker intensity of rainfall anomaly compared to the observation in the composite of the El Niño/La Niña events. (Fig. 7q,r). During DJF, the SE Asia region has a weaker ENSO connection compared to that of the other 3 seasons (Fig. 7c). Observations do not show any significant correlation except over the Philippines and northeast region of Kalimantan Island. The model is able to simulate these correlations with ENSO but with weak intensity. The correlation map (Fig. 7s,v) reflects in the composite rainfall anomaly of El Niño and La Niña years, but the model erroneously simulates excess rainfall over southern Sumatra and southwest Kalimantan.

The above discussion indicates that the model is able to simulate the spatio-temporal variability of rainfall in relation to ENSO, although there are some biases. For example, the model captures the negative ENSO correlation over the Indonesian region during JJA and SON, though model has weaker intensity during SON. The model also captures the ENSO connection over the smaller region of SE Asia during the DJF season. The only exception is that the model
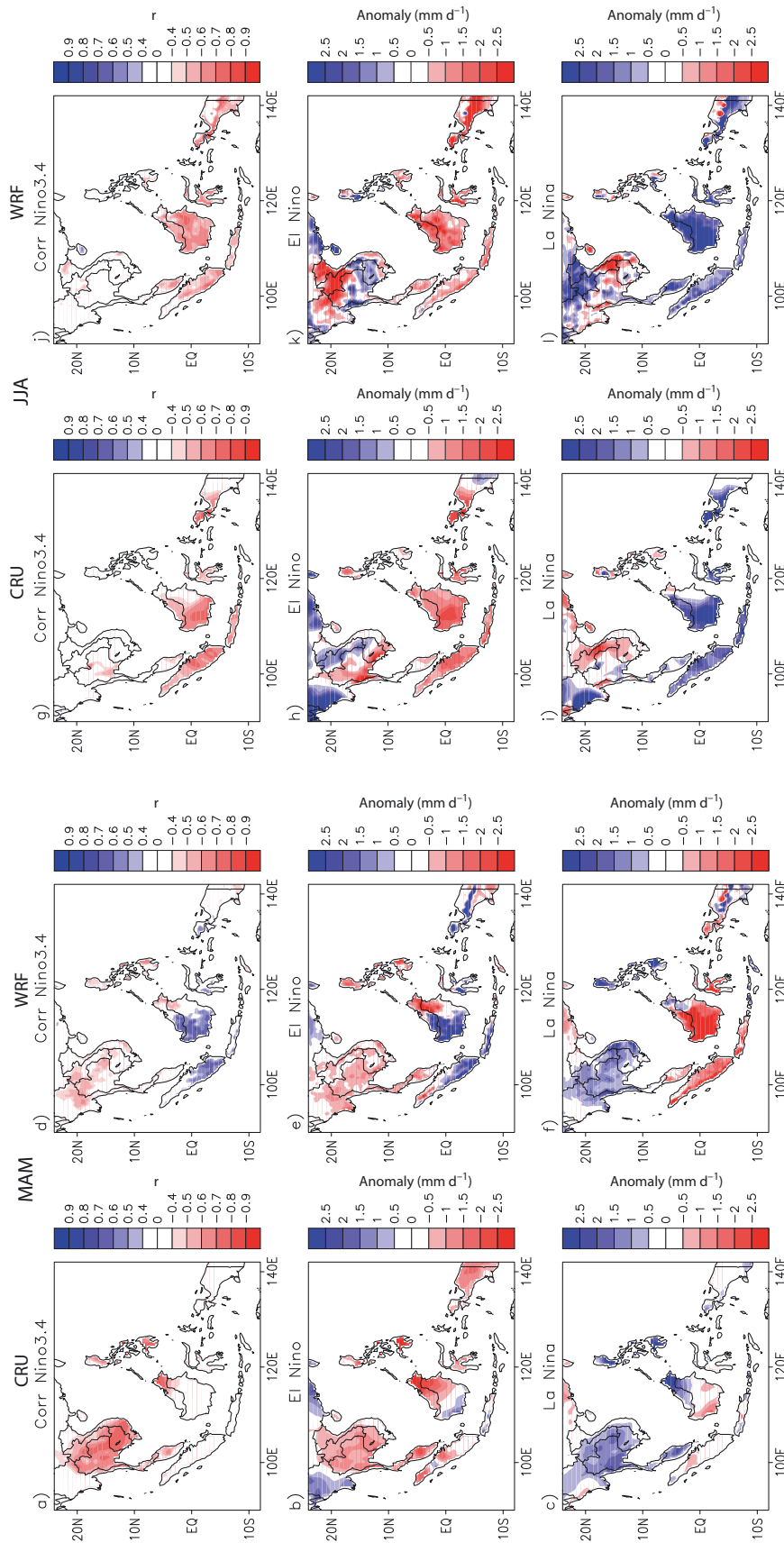
Fig 7. (a,d) Correlation coefficient between MAM mean Niño 3.4 index and MAM mean rainfall anomalies for the 25 yr (1991–2015) period both for CRU and WRF data. (b,c) CRU composite rainfall anomaly (mm d⁻¹) for the MAM season during El Niño and La Niña respectively. (e,f) Same as (b,c) but using WRF simulated composite anomaly. (g–l) Same as (a–f) but for JJA season; (m–r) same but for SON season; (s–x) same but for DJF season. Correlation coefficient values shown are statistically significant at 95% level with 2-tailed Student's t-test
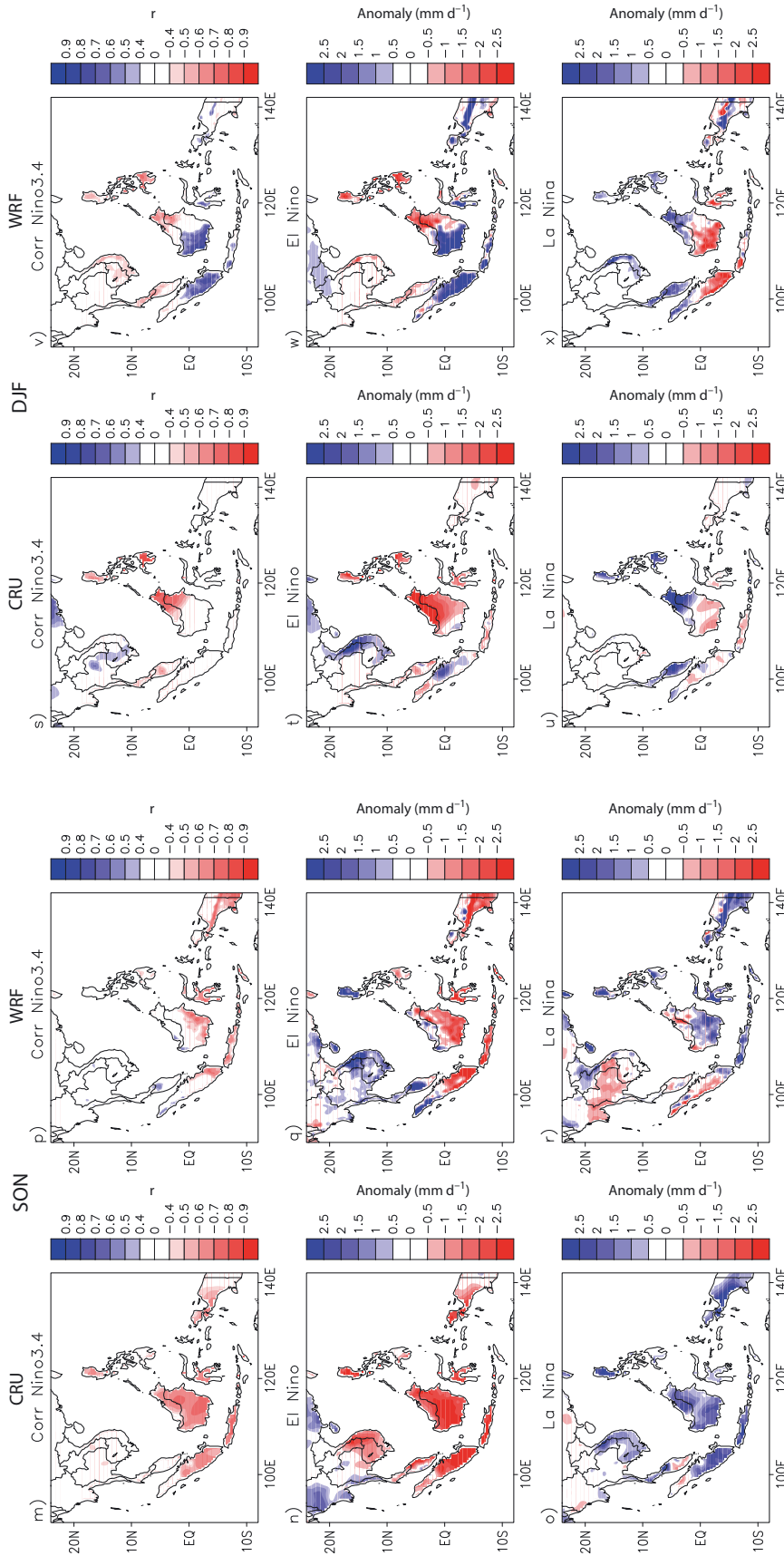
Fig 7. (continued)

incorrectly simulates a positive ENSO correlation over Indonesia region during MAM and DJF. This incorrect correlation with ENSO over the Indonesian region in these particular seasons is responsible for the weak correlation (Table 2) between observations and modelled seasonal rainfall at an interannual scale during the study period of 25 yr.

To further check if the model simulates the divergence and circulation processes realistically during the El Niño and La Niña, we analyzed the composite anomaly of divergence and wind vectors at 850 hPa during the El Niño and La Niña years (Fig. 8). In this SE Asia sector, the evolution of anomalous 850 hPa winds is strongly linked to the evolution of SST during ENSO and IOD events, as discussed in the rich literature (Wang et al. 2003, Juneng & Tangang 2005, Ummenhofer et al. 2013, Tsai et al. 2015). The divergence and circulation patterns were analyzed for all the seasons of the year, but we here show those only for JJA and SON because of the strong influence of ENSO on the seasonal rainfall. The composite anomaly of divergence analysis in JJA shows divergence over the Indonesian region during El Niño years and convergence during La Niña years (Fig. 8a,b). The model successfully simulated the divergence over Indonesia during El Niño years, but the simulated convergence during La Niña is stronger than the observed convergence (Fig. 8c,d), which can be seen from the bias of divergence (Fig. 8e,f). The stronger convergence of wind over the Indonesian region during La Niña (Fig. 8d) contributes to excess rainfall (Fig. 7l) compared to the observations. Also, the difference between the model and observation (Fig. 8e) shows an anomalous cyclonic circulation over the Philip-

Table 3. Correlation of ENSO and IOD with the area averaged rainfall for different subregions of SE Asia. *Statistically significant at 95% level with 2-tailed Student's *t*-test

		MAM	JJA	SON	DJF
ENSO					
MLS	CRU	−0.62*	−0.03	−0.24	0.29
	WRF	−0.55*	−0.13	0.09	−0.10
MSI	CRU	−0.27	−0.76*	−0.79*	−0.48*
	WRF	0.64*	−0.70*	−0.40*	0.54*
PHS	CRU	−0.86*	−0.02	−0.74*	−0.81*
	WRF	−0.70*	−0.12	−0.33	−0.77*
EIT	CRU	−0.23	−0.71*	−0.64*	−0.23
	WRF	0.35	−0.83*	−0.76*	0.39*
IOD					
MLS	CRU	0.42*	0.14	−0.00	−0.07
	WRF	0.24	0.03	0.04	−0.13
MSI	CRU	0.54*	−0.23	−0.84*	−0.23
	WRF	−0.37	−0.35	−0.47*	0.04
PHS	CRU	0.37*	0.22	−0.69*	−0.21
	WRF	0.19	−0.13	−0.39*	−0.10
EIT	CRU	0.05	−0.06	−0.52*	−0.25
	WRF	−0.43*	−0.38	−0.66*	0.22

pines during El Niño years, which generates a positive rainfall anomaly compared to the negative rainfall anomaly observed. Similar characteristics of divergence and convergence are also observed during the SON season (Fig. 8g,h), and the model successfully simulated these features (Fig. 8i,j). The simulated anomalous convergence over the MLS and PHS regions during El Niño years (Fig. 8k) contributed to excess rainfall compared to the observations (Fig. 7n,q).

4.2. SE Asia rainfall variability and IOD

The IOD is also known to influence the climate of SE Asia because this region is located near the eastern pole of the IOD. To understand the influence of the IOD with rainfall over SE Asia in a regional climate model, we calculated the correlation coefficient between the IOD index and rainfall for the 4 seasons MAM, JJA, SON, and DJF for the period 1991 to 2015 using the observed and model simulated data (Table 3b). Except for the MLS region, IOD has the strongest influence on the SE Asia rainfall variability during the SON season compared to the other 3 seasons, clearly due to the IOD peaking in the boreal autumn season (Saji et al. 1999). Therefore, further analysis with IOD is carried out only for the SON season. The model successfully simulates this IOD and rainfall relationship, but the simulated

correlation is generally weaker compared to that observed (Table 3b).

The observed rainfall shows the strongest negative correlation with IOD during the SON season over the Indonesian region, and a weak negative correlation over the PHS region (Fig. 9). The IOD is known to peak during the SON season (Saji et al. 1999), and Indonesia receives deficient (excess) rainfall anomaly during positive (negative) IOD years. The model also simulates these rainfall anomalies with respect to the positive and negative IOD, but with a somewhat weaker amplitude. The model successfully simulates the negative rainfall anomaly over the MSI region, associated with positive IOD years in 1994 and 1997, but fails to simulate the excess rainfall anomaly during the negative IOD years of 1996 and 1998. However, the model is successful in simulating the positive rainfall anomaly for the 2010 negative IOD event (see Fig. 6c).

The performance of the WRF model was also checked to see whether it can simulate the 850 hPa divergence and circulation patterns over SE Asia associated with IOD events during SON season. There is strong divergence over SE Asia, with strong easterly winds over southwestern region of Indonesia during positive IOD events (Fig. 10a). These winds diverge over the Indonesian region with a cold SST anomaly, and converge over the western Indian Ocean due to a warm SST anomaly there (not shown). This divergence over the Indonesian region causes a negative rainfall anomaly during the positive IOD events. During the negative IOD years, an anomalous convergence zone is observed over SE Asia, and this causes a anomalous excess rainfall during negative IOD years. The model-simulated divergence is weaker than that observed during positive IOD events (Fig. 10c,e), but the convergence of winds from west and east is well simulated by the model during the negative IOD years (Fig. 10d,f). The model simulations have an anomalous cyclonic circulation bias over southern MLS, Malaysia, and north Sumatra (Fig. 10e) during positive IOD years, and hence, the model simulates a wet rainfall anomaly compared to that observed.

5. SUMMARY

To verify the performance of the WRF model in reproducing the regional climate variability over SE Asia, we conducted a 25 yr (1991–2015) model simulation at 27 km horizontal resolution using the European Centre for Medium-Range Weather Forecasts
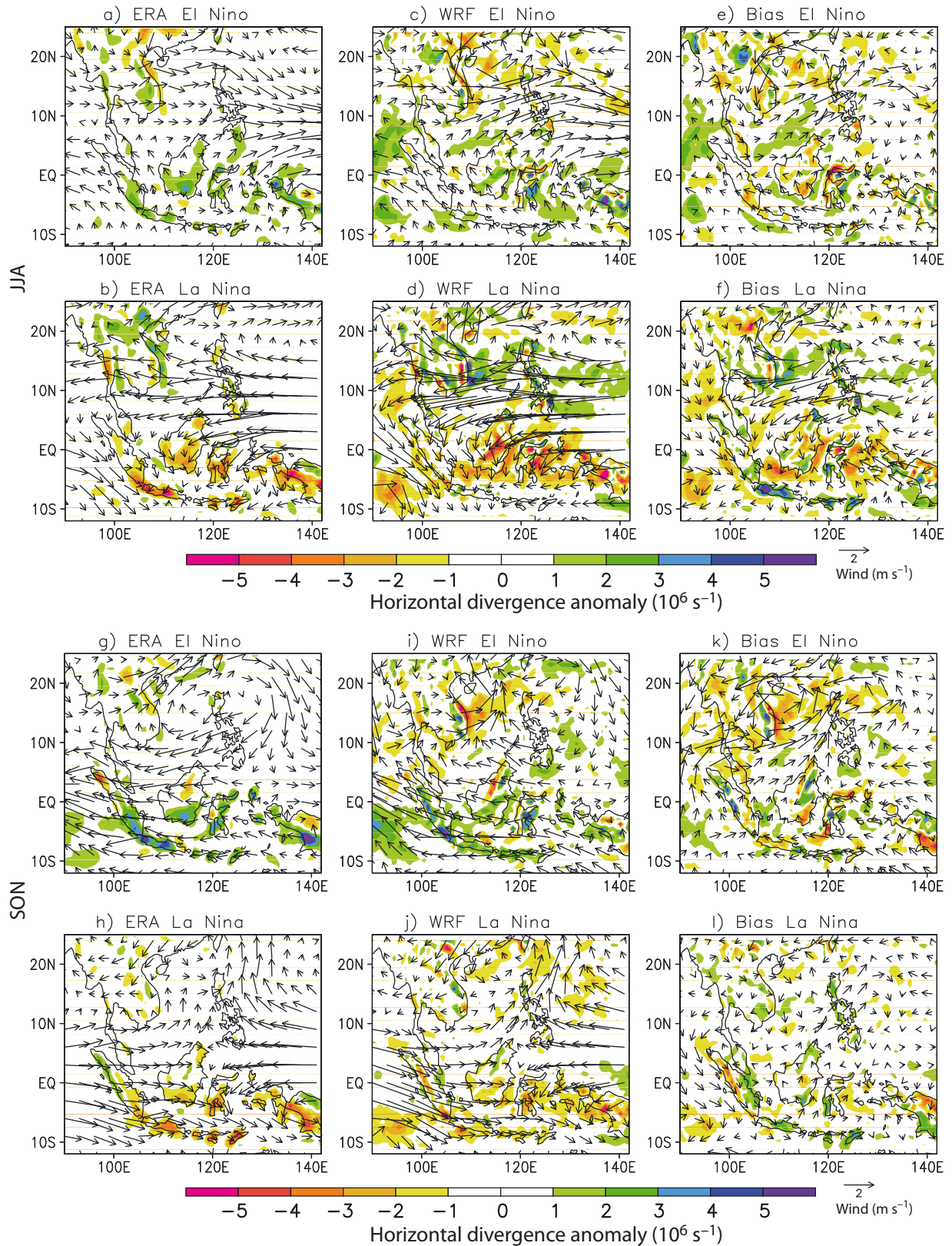
Fig. 8. (a–d) JJA mean composite anomaly of horizontal divergence (color) and winds (vectors) at 850 hPa for El Niño and La Niña events using (a,b) ERA and (c,d) WRF data. (e,f) Bias as calculated from the difference between WRF and ERA data for the El Niño and La Niña events, respectively. (g–l) same as (a–f) but for SON composite anomaly
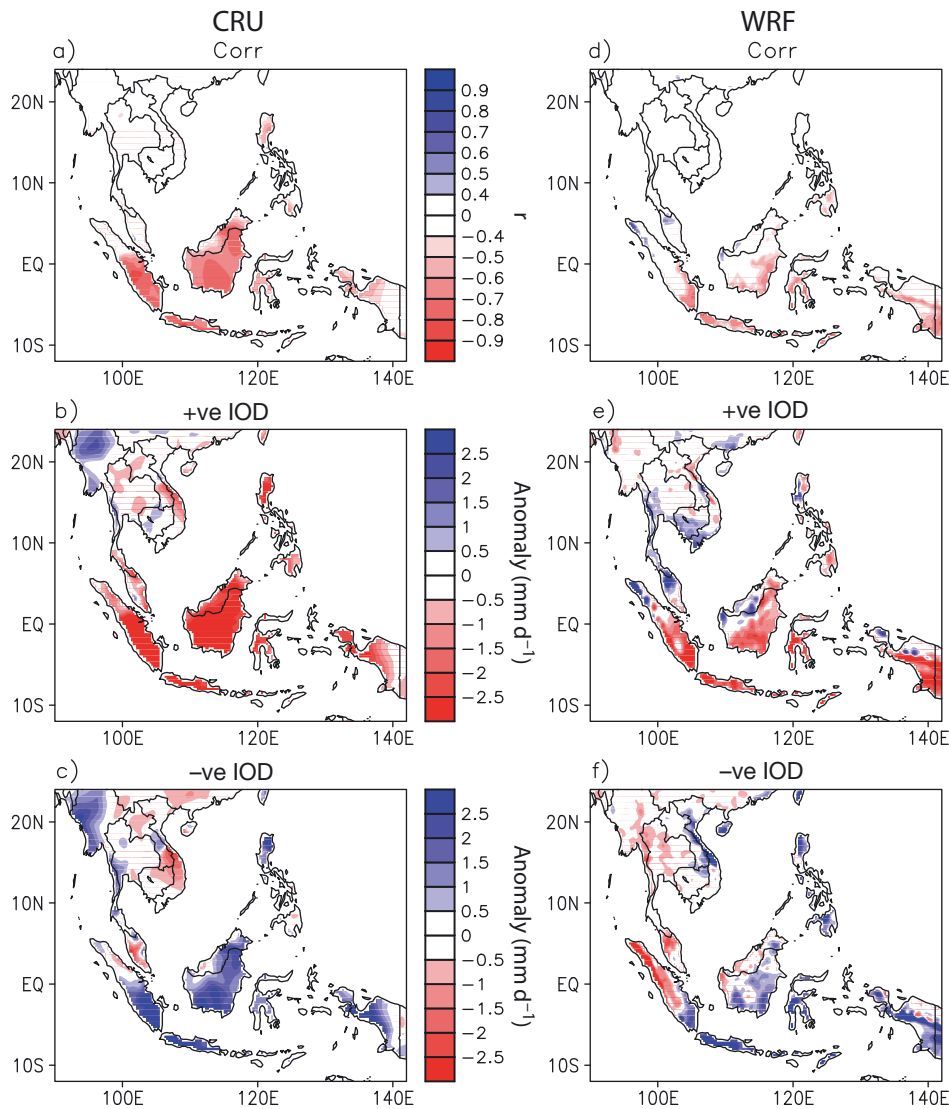
Fig 9. (a,d) Correlation coefficient between SON mean IOD index and SON mean rainfall for the 25 yr (1991–2015) period for CRU (left column) and WRF (right column) data. (b,c,e,f) Composite rainfall anomaly for the MAM season during positive and negative IOD events. (e,f) Same as (b,c) but using WRF simulated composite anomaly. Correlation coefficient values shown are statistically significant at 95% level with 2-tailed Student's *t*-test

(ECMWF) reanalysis (ERA-Interim) data as the forcing boundary data. We checked the fidelity of the model in reproducing the climatology, annual cycle, and interannual variability of rainfall for the different subregions of SE Asia during 4 seasons (MAM, JJA, SON, and DJF). The rainfall variability over SE Asia with relation to large-scale climate modes such as ENSO and IOD was also analyzed.

The results indicate that the model simulates the spatial variability and annual rainfall climatology with maximum rainfall over Malaysia and Indonesia and minimum rainfall over mainland SE Asia and the Philippines. However, we found a dry bias over the western coast of Myanmar, Malaysia, and parts of the

Kalimantan Island and a wet bias over eastern part of MLS, western Sumatra, and the Philippines. Based on analyzing the individual seasons, the model simulates a wet bias over MLS region (except Myanmar) during JJA. The analysis of the climatology of the vertically integrated moisture flux indicates that excess moisture convergence over the MLS and PHS during JJA season contributes to the excess rainfall. Compared to observations, the model simulated a weaker moisture flux along the Myanmar coast, and hence generated a dry bias in orographic rainfall. The dry bias simulated over Malaysia, northern Sumatra, and parts of Kalimantan Island in the annual climatology comes from the strong bias during DJF.
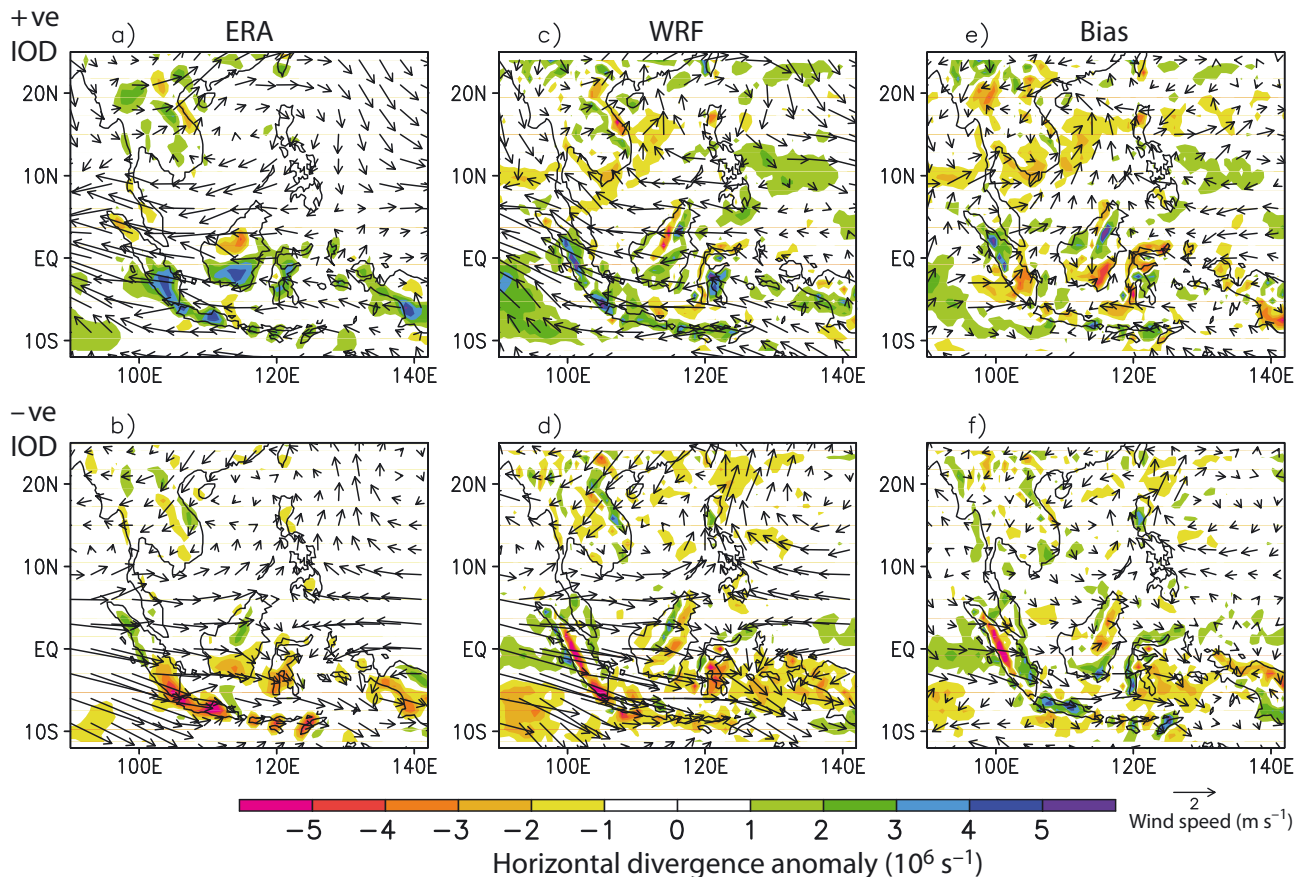
Fig. 10. (a−d) SON mean composite anomaly of horizontal divergence (color) and winds (vectors) at 850 hPa for positive IOD and negative IOD events using (a,b) ERA and (c,d) WRF data. (e,f) Bias, calculated as the difference between WRF and ERA data for the positive IOD and negative IOD events, respectively

The moisture convergence zones shift over the Indonesia region during the DJF season with the movement of the ITCZ southward. The model simulates weaker moisture convergence compared to the observation results in dry bias during DJF. The vertical profile of moisture and vertical velocity bias is also reflected in the wet (dry) bias over the MLS (MSI) region during JJA (DJF).

This study also evaluates the WRF model's ability to simulate the interannual variability of regional rainfall over SE Asia, and its association with the large-scale climate modes, such as ENSO and IOD. Due to its location, the maritime continent is influenced by both the ENSO and IOD. On an interannual scale, the model performs well over mainland SE Asia and the Philippines for all seasons of the year except for the boreal summer (JJA). In general, this is the region where ENSO has very little correlation during JJA, and the model successfully simulated the low correlation between rainfall and the Niño 3.4 index. In contrast, the model has good skill over the MSI region during the boreal summer compared to

the other 3 seasons. The Indonesian region has a strong ENSO influence during the boreal summer season, and the model accurately reproduces the rainfall and Niño 3.4 correlation. Also, the model shows good performance in the EIT region during both the boreal summer and fall seasons. The model is able to realistically capture SON rainfall over the Indonesian region during IOD events. During the SON season, both IOD and ENSO have stronger influences over the Indonesia region, but the model reproduces only a weak but significant negative correlation (rainfall–ENSO and rainfall–IOD) compared to the strong correlation in the observation. The accurate representation of the relationship between rainfall and ENSO/IOD is due to the model's ability to realistically simulate the large-scale circulation patterns. This indicates that the WRF model could reproduce the spatio-temporal variability of rainfall with relation to ENSO and IOD.

The WRF model simulates the seasonal climatology and annual cycle, and captures the interannual variability reasonably well over all the subregions of the

SE Asia. However, the model suffers from severe systematic biases of overestimating (underestimating) precipitation during peak rainfall seasons over the MLS (MSI) region. Further experiments with various combination of physical parameterization schemes together with air–sea interactions (e.g. Wei et al. 2014) are needed to reduce these biases. We intend to carry out such experiments in the future.

LITERATURE CITED

Adler RF, Huffman GJ, Chang A, Ferraro R and others (2003) The version 2 global precipitation climatology project (GPCP) monthly precipitation analysis (1979-present). J Hydrometeorol 4:1147–1167

Aldrian E, Dumenil-Gates L, Jacob D, Podzun R, Gunawan D (2004) Long-term simulation of Indonesian rainfall with the MPI regional model. Clim Dyn 22:795–814

Behera SK, Luo JJ, Yamagata T (2008) The unusual IOD event of 2007. Geophys Res Lett 35:L14S11

Betts AK, Miller MJ (1986) A new convective adjustment scheme. II. Single column tests using GATE wave, BOMEX, and arctic air-mass data sets. QJR Meteorol Soc 112:693–709

Chen F, Dudhia J (2001) Coupling an advanced land-surface hydrology model with the Penn State-NCAR MM5 modeling system. I. Model implementation and sensitivity. Mon Weather Rev 129:569–585

Chotamonsak C, Salathe EP Jr, Kreasuwan J, Chantara S, Siriwitayakorn K (2011) Projected climate change over Southeast Asia simulated using a WRF regional climate model. Atmos Sci Lett 12:213–219

Chotamonsak C, Salathe EP Jr, Kreasuwan J, Chantara S (2012) Evaluation of precipitation simulations over Thailand using a WRF regional climate model. Warasan Khana Witthayasat Maha Witthayalai Chiang Mai 39: 623–638

Dee DP, Uppala SM, Simmons AJ, Berrisford P and others (2011) The ERA-interim reanalysis: configuration and performance of the data assimilation system. QJR Meteorol Soc 137:553–597

Dickinson RE, Errico RM, Giorgi F, Bates GT (1989) A regional climate model for the western United States. Clim Change 15:383–422

Dudhia J (1989) Numerical study of convection observed during the winter monsoon experiment using a mesoscale two-dimensional model. J Atmos Sci 46: 3077–3107

Francisco RV, Argete J, Giorgi F, Pal J, Bi X, Gutowski W (2006) Regional model simulation of summer rainfall over the Philippines: effect if choice of driving fields and ocean flux schemes. Theor Appl Climatol 86:215–227

Giorgi F (1990) Simulation of regional climate using a limited area model nested in a general circulation model. J Clim 3:941–963

Giorgi F, Mearns LO (1999) Introduction to special section: regional climate modelling revisited. J Geophys Res 104: 6335–6352

Giorgi F, Bi X, Pal JS (2004) Mean, interannual variability and trends in a regional climate change experiment over Europe. I. Present-day climate (1961–1990). Clim Dyn 22:733–756

Harris I, Jones PD, Osborn TJ, Lister DH (2014) Updated high-resolution grids of monthly climatic observations–the CRU TS3.10 dataset. Int J Climatol 34:623–642

Hong SY, Dudhia J, Chen SH (2004) A revised approach to ice microphysical processes for the bulk parameterization of clouds and precipitation. Mon Weather Rev 132: 103–120

Huffman GJ, Adler RF, Bolvin DT, Gu GJ and others (2007) The TRMM Multisatellite Precipitation Analysis (TMPA): quasi-global, multiyear, combined-sensor precipitation estimates at fine scales. J Hydrometeorol 8:38–55

Im ES, Ahn JB, Remedio AB, Kwon WT (2008) Sensitivity of the regional climate of East/Southeas Asia to convective parameterizations in the RegCM3 modelling system. 1. Focus on the Korean peninsula. Int J Climatol 28: 1861–1877

Janjic ZI (1994) The step-mountain eta coordinate model: further developments of the convection, viscous sublayer and turbulence closure schemes. Mon Weather Rev 122: 927–945

Juneng L, Tangang FT (2005) Evolution of ENSO-related rainfall anomalies in Southeast Asia region and its relationship with atmosphere–ocean variations in Indo-Pacific sector. Clim Dyn 25:337–350

Juneng L, Tangang F, Chung JX, Ngai ST and others (2016) Sensitivity of the Southeast Asia rainfall simulations to cumulus and ocean flux parameterization in RegCM4. Clim Res 69:59–77

Kripalani RH, Kulkarni A (1997) Rainfall variability over South-east Asia: connections with Indian monsoon and ENSO extremes: new perspective. Int J Climatol 17: 1155–1168

Lau KM, Yang S (1997) Climatology and interannual variability of the southeast Asian summer monsoon. Adv Atmos Sci 14:141–162

Li JP, Zeng QC (2005) A new monsoon index, its interannual variability and relation with monsoon precipitation. Clim Environ Res 10:351–365

Liew SC, Raghavan SV, Liong SY (2014) Development of Intensity-Duration-Frequency curves at ungauged sites: risk management under changing climate. Geosci Lett 1:8

Matsumoto J, Murakami T (2002) Seasonal migration of monsoons between the northern and southern hemisphere as revealed from equatorially symmetric and asymmetric OLR data. J Meteorol Soc Jpn 80:419–437

McBride J, Haylock M, Nicholls N (2003) Relationship between the maritime continent heat source and the El Niño–Southern oscillation phenomenon. J Clim 16: 2905–2914

Mlawer E, Taubman S, Brown P, Iacono M, Clough S (1997) Radiative transfer for inhomogeneous atmosphere: RRTM,

a validated correlated-k model for the long-wave. J Geophys Res 102:16663–16682

Naylor RL, Battisti DS, Vimont DJ, Falcon WP, Burke MB (2007) Assessing risks of climate variability and climate change for Indonesian rice agriculture. Proc Natl Acad Sci USA 104:7752–7757

Ngo-Duc T, Kieu C, Thatcher M, Nguyen-Le D, Phan-Van T (2014) Climate projections for Vietnam based on regional climate models. Clim Res 60:199–213

Noh Y, Cheon WG, Hong SY, Raasch S (2003) The improvement of the K-profile model for the PBL using LES. Boundary-Layer Meteorol 107:401–427

Phan VT, Ngo-Duc T, Ho TMH (2009) Seasonal and interannual variations of surface climate elements over Vietnam. Clim Res 40:49–60

Phan VT, Nguyen HV, Tuan LT, Quang TN, Ngo-Duc T, Laux P, Xuan TN (2014) Seasonal prediction of surface air temperature across Vietnam using the regional climate model version 4.2 (RegCM4.2). Adv Meteorol 2014:245104

Raghavan SV, Vu MT, Liong SY (2016) Regional climate simulations over Vietnam using the WRF model. Theor Appl Climatol 126:161–182

Raktham C, Bruyère C, Kreasuwun J, Done J, Thongbai C, Promnopas W (2015) Simulation sensitivities of the major weather regimes of the Southeast Asia region. Clim Dyn 44:1403–1417

Ratna SB, Ratnam JV, Behera SK, Rautenbach CJ, Ndarana T, Takahashi K, Yamagata T (2014) Performance assessment of three convective parameterization schemes in WRF for downscaling summer rainfall over South Africa. Clim Dyn 42:2931–2953

Ratna SB, Cherchi A, Joseph PV, Behera SK, Abish B, Masina S (2016a) Moisture variability over the Indo-Pacific region and its influence on the Indian summer monsoon rainfall. Clim Dyn 46:949–965

Ratna SB, Ratnam JV, Behera SK, Doi T, Yamagata T (2016b) Downscaled prediction of extreme seasonal climate over Southeast Asia using a regional climate model. Techno-Ocean 2016, IEEE Kobe, p 375–380

Reynolds RW, Rayner NA, Smith TM, Stokes DC, Wang W (2002) An improved in situ and satellite SST analysis for climate. J Clim 15:1609–1625

Saji NH, Goswami BN, Vinayachandran PN, Yamagata T (1999) A dipole mode in the tropical Indian Ocean. Nature 401:360–363

Salimun E, Tangang F, Juneng L, Behera SK, Yu W (2014) Differential impacts of conventional El Niño versus El Niño Modoki on Malaysian rainfall anomaly during winter monsoon. Int J Climatol 34:2763–2774

Skamarock WC, Klemp JB, Dudhia J, Gill DO and others (2008) A description of the advanced research WRF version 3. NCAR technical note, NCAR/TN\u2013475?STR, Boulder, CO

Takahashi HG, Yoshikane T, Hara M, Yasunari T (2009) High resolution regional climate simulations of the long-term decrease in September rainfall over Indochina. Atmos Sci Lett 10:14–18

Takahashi HG, Yoshikane T, Hara M, Takata K, Yasunari T (2010) High resolution modeling of the potential impact of land surface conditions on regional climate over Indochina associated with diurnal precipitation cycle. Int J Climatol 30:2004–2020

Tangang F, Juneng L (2004) Mechanisms of Malaysian rainfall anomalies. J Clim 17:3616–3622

Tsai C, Behera SK, Waseda T (2015) Indo-China monsoon indices. Sci Rep 5:8107

Ummenhofer CC, D'Arrigo RD, Anchukaitis KJ, Buckley BM, Cook ER (2013) Links between Indo-Pacific climate variability and drought in the Monsoon Asia Drought Atlas. Clim Dyn 40:1319–1334

Wang B, Wu R, Li T (2003) Atmosphere–warm ocean interaction and its impacts on Asian–Australian monsoon variation. J Clim 16:1195–1211

Wei J, Malanotte-Rizzoli P, Eltahir EAB, Xue P, Xu D (2014) Coupling of a regional atmospheric model (RegCM3) and a regional ocean model (FVCOM) over the Maritime Continent. Clim Dyn 43:1575–1594

Yatagai A, Kamiguchi K, Arakawa O, Hamada A, Yasutomi N, Kitoh A (2012) APHRODITE: constructing a long-term daily gridded precipitation dataset for Asia based on a dense network of rain gauges. Bull Am Meteorol Soc 93: 1401–1415

Yusuf AA, Francisco HA (2009) Climate change vulnerability mapping for Southeast Asia. Economy and Environment Program for Southeast Asia (EEPSEA), Singapore

Zeng Q, Zhang B (1998) On the seasonal variation of atmospheric general circulation and the monsoon. Chinese J Atmos Sci 22:805–813 (in Chinese)